sustainability

MDPI

Article

Effect of Phase Change Materials (PCMs) Integrated into a Concrete Block on Heat Gain Prevention in a Hot Climate

Ahmad Hasan *, Khaled A. Al-Sallal, Hamza Alnoman, Yasir Rashid and Shaimaa Abdelbaqi

College of Engineering, United Arab Emirates University, P.O. Box, Al Ain 15551, UAE; k.sallal@uaeu.ac.ae (K.A.A.-S.); ha1987@uaeu.ac.ae (H.A.); yasir.rashid@uaeu.ac.ae (Y.R.); 200734406@uaeu.ac.ae (S.A.)

* Correspondence: ahmed.hassan@uaeu.ac.ae; Tel.: +971-56-8695917

Academic Editor: Andrew Kusiak

Received: 14 August 2016; Accepted: 21 September 2016; Published: 10 October 2016

Abstract: In the current study, a phase change material (PCM) contained in an insulated concrete block is tested in extremely hot weather in the United Arab Emirates (UAE) to evaluate its cooling performance. An insulated chamber is constructed behind the block containing PCM to mimic a scaled down indoor space. The effect of placement of the PCM layer on heat gain indoors is studied at two locations: adjacent to the outer as well as the inner concrete layer. The inclusion of PCM reduced heat gain through concrete blocks compared to blocks without PCM, yielding a drop in cooling load indoors. The placement of PCM and insulation layers adjacent to indoors exhibited better cooling performance compared to that adjacent to the outdoors. In the best case, a temperature drop of 8.5% and a time lag of 2.6 h are achieved in peak indoor temperature, rendering a reduction of 44% in the heat gain. In the tested hot climate, the higher ambient temperature and the lower wind speed hampered heat dissipation and PCM re-solidification by natural ventilation. The findings recommend employing a mechanical ventilation in hot climates to enhance regeneration of the PCM to solid state for its optimal performance.

Keywords: phase change material; thermal management; building insulations; air infiltration; time lag; decrement factor

1. Introduction

World energy consumption increased two-fold from 1973 to 2012, reaching up to 8500 Mtoe (million tons of oil equivalent) [1]. This has resulted in an increase of greenhouse gas emissions by 7.7% from 1990 to 2014 [2]. In the European Union, 40% of the total energy is consumed by buildings for heating, cooling, and ventilation and is expected to increase further in future [3]. Out of the total energy consumed by buildings in Canada, 81% is consumed by residential buildings mainly for space and water heating needs [4]. The huge amount of energy consumption directly contributes to carbon dioxide emissions leading to the greenhouse effect resulting in climate change [5]. In order to avoid climate change, zero carbon homes becoming a target [6], mainly by passive means. In order to meet the target of zero energy homes by avoiding excessive heat gain/loss, multi-layered insulated and single-layered walls are being designed [7]. By selecting appropriate coating materials for the outer surface of a wall, its absorption coefficient can be tuned inducing a time lag in the heat gain and a drop in temperature swing [8]. The induced time lag further increases with the increase in thermal inertia of the building materials [9]. Building envelopes with a higher thermal inertia are considered to be more energy efficient specifically in a higher heat load condition [10,11]. Integration of phase change materials (PCMs) into the building envelope [12] is increasingly replacing conventional, costlier, and massive construction techniques [13], intended to increase thermal inertia. PCMs have

been integrated into building materials by direct immersion into concrete blocks, direct mixing into insulations or integrating of micro-capsulated PCMs into concrete aggregates. Direct immersion causes leakage of PCMs and moisture transfer problems; therefore, it is being increasingly discarded [14]. Direct mixing of PCMs in insulation causes evaporation (in the case of inorganic PCMs), degradation, and eventual dematerialization (in the case of organic PCMs) [15], leading to failures. Integration of microencapsulated PCMs into the concrete aggregate causes uneven distribution of PCM inside the concrete, thereby creating structural failures [16].

PCMs have been applied to building skin in different configurations as shown in Figure 1A–E. Through a numerical model, a single PCM layer was optimized for the climatic conditions of Quebec City, Canada, as shown in Figure 1A. The study reported that PCM is functional only when there exists a lesser temperature difference between outdoors and indoors [17]. A sandwich wall configuration as shown in Figure 1B [18] was studied to determine the effect of the melting point of PCMs on energy saving. The research resulted in finding optimum melting points for various outdoor conditions. A wall section as presented in Figure 1C evaluated in winter and summer conditions of the UK through numerical simulation reported that a 20 mm thick PCM layer along with a 20 mm air cavity can optimally achieve thermal comfort indoors [19]. A PCM vertical layer as shown in Figure 1D applied to south and west walls damped peak heat flux by 51% and 30%, delayed peak time by 6.3 h and 2.3 h, and reduced heat transfer by 27% and 4%, respectively [20]. A PCM based thermal energy storage (PCMTS) as shown in Figure 1E performed optimally when placed inwards next to the gypsum wallboard, yielding an 11% reduction in heat flux in Kansas, USA [21]. A PCM configuration as shown in Figure 1F reported a temperature drop of 7 °C and a time lag of 6 h at maximum in the typical weather conditions of Tlemcen (western Algeria) [22].

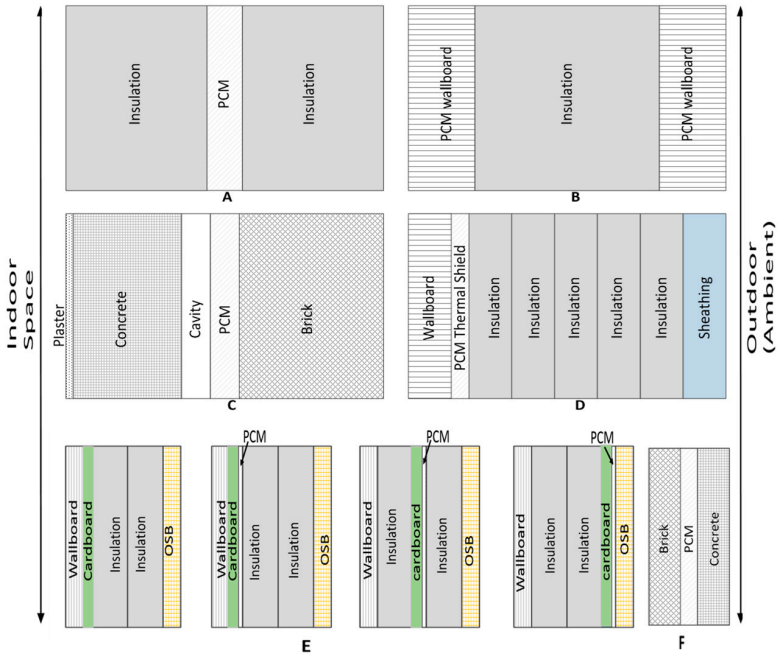

Figure 1. Previously investigated configurations of integrating phase change materials (PCMs) in wall sections, namely: (**A**) a thin layer of PCM between two layers of insulation tested in Quebec City, Canada [17]; (**B**) two layers of PCM impregnated wallboards applied as an exterior and an interior layer with thick insulation in-between, tested in a continental climate [18]; (**C**) a PCM and an air cavity layer contained between two concrete blocks, tested in the cold climate of South East England, UK [19]; (**D**) a PCM layer installed near the internal wallboard having multi-layers of insulation boards and sheathing towards the exterior, tested in Kansas, USA [20]; (**E**) various configurations of gypsum wallboard, cardboard, PCM layer, insulation layer and OSB layer, tested in Kansas, USA [21]; and (**F**) a simple wall assembly of brick and concrete, applying a PCM layer in-between, tested in West Algeria [22].

In the case where the cavity was filled in with microencapsulated PCM, conduction was found to be the dominant mode of heat transfer during melting and solidification, which renders a drop in sub-cooling effect compared to one free from PCMs [23]. Microencapsulated PCM-filled floor cavities studied experimentally and numerically yielded a drop in indoor temperature swing by 1 °C [24]. Integration of PCM in the building facades yielded an increased heat storage capacity of 2501.3 kJ in 24 h, resulting in an increase in the indoor temperature in the colder climates of Coimbra [25]. Integration of PCM with air cavities in the attic roof employing a building-integrated photovoltaic system reduced the roof-generated heating load by 30% in the winter and cooling load by 55% in the summer [26]. For a wall outfitted with PCM, the space-cooling load was reduced by 10.4%, rendering a 7.2% drop in annual energy consumption [27]. Cooling/heating performance of the PCM heavily depends on its melting and solidification characteristics [28], placement [29], and the presence of an air cavity adjacent to the PCM layer [30]. Some studies suggest that the PCM melting point should be up to 3 °C higher than the required indoor temperature [31]. Others recommend it to be near indoor temperature to minimize thermal load [32]. Recent studies have linked PCM melting point to nighttime ambient temperatures in order to regenerate the PCM passively at night in hot climates [33].

Summarizing the previous studies, PCM solidus temperature (T_s) is desired to be higher than the average ambient temperature during the nighttime of the summer months. This measure would allow the PCM to release heat to ambient levels and get back to solid in critical summer conditions. After reviewing Al Ain weather data from a climate consultant, $T_{amb\text{-}avg\text{-}nig}$ in summer months was found to be 34 °C. The PCM properties were compared to determine an optimum PCM type for the experiment. It was found that the paraffin waxes possess thermal conductivity (0.2 W/m·K) comparable to fatty acids (0.14 W/m·K) and lower than salt hydrates (1.08 W/m·K); heat of fusion (139 kJ/kg) comparable to salt hydrates (210 kJ/kg) and fatty acids (168 kJ/kg); density (0.88 kg/m^3) comparable to fatty acids (0.89 kg/m^3) and lower than salt hydrates (1.7 kg/m^3). Paraffins showed no sub-cooling, while the salt hydrates and fatty acids do show a stronger and a mild sub-cooling, respectively. Paraffins were not corrosive to metals while salt hydrates and fatty acids do show corrosion to the metals [33].

The current research investigates the effect of melting point and placement location of the PCM on its cooling performance in the extremely hot weather conditions of UAE. Based on the criteria suggested in the literature [34], a PCM was selected with the melting point of 37 °C, being higher than the average nighttime ambient temperature in summer (35.3 °C) in Al Ain, UAE. A layer of the PCM is added into a concrete block attached to a small, insulated cubic chamber representing the indoor space.

2. Materials and Methods

The research methodology entails the integration of a PCM into a concrete block in two arrangements to study its cooling effect in extremely hot weather conditions. Heat stored in the melted PCM is removed by natural convection through an air cavity. The cooling effect produced by the PCM is quantified by temperature changes on the front and the back surfaces of the wall and ambient air indoors. Cooling load saving achieved by inclusion of the PCM is represented by a reduced heat transfer rate and a time lag in the peak indoor temperature.

2.1. Selection of Experimental Parameters

Three concrete blocks, one without PCM (block A) and the other two containing PCM (block B and block C), are used in the experiment to compare their thermal performance as shown in Figure 2. The thickness of the concrete, the PCM and the insulation layer is 2.5 cm, 5 cm and 1 cm, respectively. A scaled down test chamber with dimensions of 40 × 40 × 40 cm^3 is constructed behind the blocks to mimic an indoor space. The test chambers are constructed from a 20 cm thick polystyrene sheet to ensure adiabatic boundary conditions. The chambers are glued through the epoxy resin to ensure impermeability. The total mass of polystyrene and epoxy is negligible compared to that of the concrete blocks and the PCM; hence their thermal energy storage capacity is ignored. The set-up was tested

outdoors in Al Ain, United Arab Emirates (latitude: 24.21° N, longitude: 55.74° E), with all the wall sections (with and without PCM) facing south direction. The thickness of the PCM layer was determined based on solar heat gain during an average summer day. It was found that a 5 cm thick paraffin-based PCM layer was enough to absorb all of the incoming solar thermal energy at the tested site.

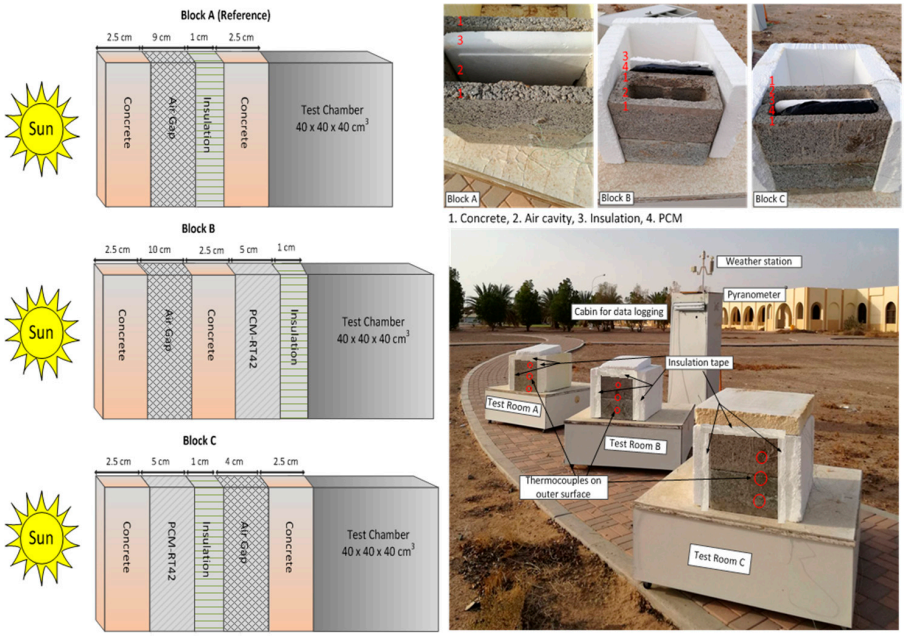

Figure 2. Schematic diagram and the experimental set-up of the concrete blocks, with construction layers and the test chamber.

2.2. Selection of the Time for Experimentation

The yearly ambient temperature was reviewed for Al Ain. Daytime and nighttime average ambient temperatures for a typical day of each month are presented in Figure 3, showing that the peak summer season spans from May to August, with similar average temperatures amongst the four months (~42 °C at day and ~35 °C at night). However, the nighttime temperature in August remained slightly higher than that of the rest of the summer months. It was therefore decided to conduct the experiment in August to study regeneration of the PCM to solid state at the warmest night, representing the worst case. It can be seen that the weather predominantly remains hot for the whole year, with average daytime temperatures being above 27 °C, the upper range of thermal comfort. Thus it was deduced that the findings for the extreme hot season would be applicable for the majority of the year.

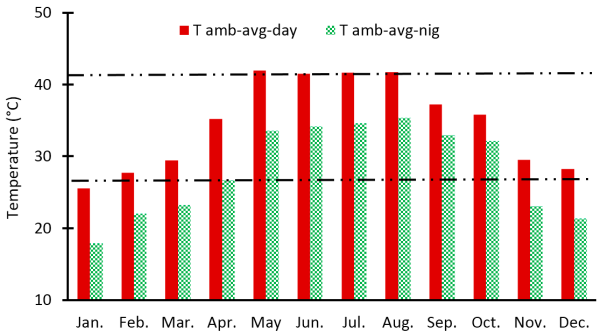

Figure 3. The measured yearly ambient temperature for a typical day of each month represented by average daytime ($T_{amb\text{-}avg\text{-}day}$) and average nighttime ($T_{amb\text{-}avg\text{-}nig}$) at the site of the experiment.

2.3. Methodology

The paraffin-based commercial PCM RT42 was melted and filled in polymer containments outfitted in an air cavity within two concrete layers. A free space for PCM solidification is left on the upside of the containment intended to accommodate volume changes and release trapped air during successive melting and solidification cycles. The fabrication materials and their thermo-physical properties are given in Table 1.

Table 1. Thermo-physical properties of the materials used in the experiments.

Properties	Melting Point (°C)	Congealing Point (°C)	Latent Heat (KJ/kg)	Specific Heat Capacity (KJ/kg·K)	Heat Conductivity (W/m·K)	Density (kg/m^3)	Volume Expansion	Flash Point (°C)
PCM-RT42 [35]	38–42	42–37	145% ± 7.5%	2	0.2	880 ^{s} 760 ^{l}	12.5%	186
Polystyrene	240	NA	NA	1.3–1.5	0.032	NA	NA	350
Epoxy Resin	130	NA	NA	1	1.26	2.09	34×10^{-6}/K	350

Note: ^{s} solid; ^{l} liquid.

Multiple t-type copper–constantan thermocouples calibrated in an ice-bath with a measurement error of ±0.3 °C were employed to m neasure temperature. The thermocouples were attached to the blocks (A, B and C) at the front surface, the back surface and inside the test chamber, as shown in Figure 4. This figure shows the setup for block C, with the same setup used for the rest of the blocks. The thermocouples were fixed with epoxy glue, shielded from direct irradiation, and monitored continuously to ensure fixation. A self-powered Apogee pyranometer (model # SP-110 with 0.2 mV per Wm^{-2} sensitivity and ±5% calibration uncertainty) [36] was installed to measure global solar radiation intensity (G). All of the sensors were connected to an NI compact Rio (NI cRIO-9073) data acquisition system having an error of 0.03% at room temperature [37]. A weather station (Starmeter-WS1041), having a temperature resolution of 0.1 °C, a temperature accuracy of ±1 °C, a wind speed measurement range of 0–50 m/s, and a wind speed resolution of 0.1 m/s, was installed to measure ambient temperature (T_{amb}) and wind speed (v_w). The temperatures were measured at the front surfaces of block A ($T_{\alpha f}$), block B ($T_{\beta f}$) and block C ($T_{\gamma f}$), at the back surfaces of block A ($T_{\alpha b}$), block B ($T_{\beta b}$) and block C ($T_{\gamma b}$), and inside the test chamber for block A ($T_{\alpha i}$), block B ($T_{\beta i}$) and block C ($T_{\gamma i}$). All the temperatures were measured at three locations and were averaged. Every measurement was logged with a time-step of 5 min since the weather is stable and no reasonable variation was observed with lesser time-steps.

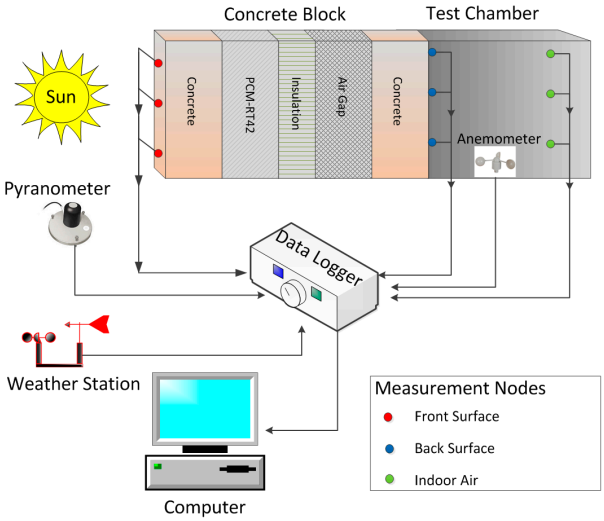

Figure 4. Schematic diagram of the experimental setup showing the configuration of block C (the same set-up is used for block A and block B).

3. Results

Experimental results of weather data, surface temperatures and indoor temperatures are presented in the following section. Peak and average values of data from 14 days are summarized in Table 2 and their mean, standard deviation (*SD*) and coefficient of variation (*CV*) are calculated to evaluate consistency and repeatability of the experiment. The results reveal that there is a repetition of the weather and resulting temperatures across different days, with marginal variations in the magnitude. In order to avoid repetition and ensure better readability, the results for one sample day (2 August 2015) are discussed along with the average of the 14 days through transient curves in Figures 5–9 (A and B), respectively. The weather data and temperatures for each day of the test duration are summarized in Table 2.

3.1. Weather Data

Figure 5 presents global solar radiation intensity (G) and wind speed (v_w) for the selected day and average of the 14 days of the experiment. Figure 5A depicts that for the sample day, the G remained fairly stable, being 230 W/m^2 at 07:00 and increasing afterwards with a stable gradient, reaching the peak value of 944 W/m^2 at 12:10. The G remained above 600 W/m^2 for 6.3 h on the selected day. A similar trend in G is observed for the average of the 14 days, with the start value of 205 W/m^2 at 07:00 and the peak value of 930 W/m^2 at 12:10 as shown in Figure 5B. Table 2 shows that the peak time G value was the highest (958 W/m^2) on day 11 and the lowest (907 W/m^2) on day three with the coefficient of variation (CV) of 2.5%, which highlights the stability of weather conditions. The fluctuations in solar radiation profile are damped when presented as an average of 14 days. Total solar energy received by the concrete surface is calculated using Equation (1).

$$Q_{in} = \sum_{i=1}^{n} G_i \times A \times \varphi \times t_i \quad (1)$$

where Q_{in} is the solar energy absorbed by concrete blocks (Wh/day), G is the global solar radiation intensity incident on the surface (W/m^2), A is the surface area of the concrete block facing south (40 × 40 cm^2), φ is the absorptance of the concrete (0.65) and t is the time in hours. The Q_{in} ranged from 679 Wh/day to 740 Wh/day between the tested days with a mean value of 709 Wh/day and CV of 1.9% as presented in Table 2.

On the sample day, v_w was 2.8 m/s at 07:00. However, it kept increasing with a varying profile afterwards, reaching the peak value of 7.2 m/s at 10:05, with a daily average value of 1.9 m/s. The v_w remained generally higher during daytime and dropped to 0 m/s at nighttime. The v_w showed daily fluctuations but exhibited a smooth profile when averaged for 14 days as shown in Figure 5B. The daily maximum and daily average v_w are presented in Table 2, with CV of 21.4% and 21.8%, respectively, representing a variable wind speed.

The wind direction is considered to be at 90° to the normal of the wall and correlations are applied pertaining to the wind speed in the range of 3 m/s to 6 m/s. Equations (2) and (3) are used to calculate the heat transfer coefficient (h_c) by applying linear and power regression [38]. The h_c is calculated to be used in Equation (4) to determine heat loss from the outer surfaces to get an insight into the wind-driven heat removal at the site. Due to a large difference in magnitude of the v_w during nighttime and daytime, the averages are calculated separately for day and night being 0.95 m/s and 2.28 m/s, respectively. The h_c remained, on average, at 9.6 W/m^2·K and 14.1 W/m^2·K for nighttime and daytime, governing heat loss and the self-cooling mechanism.

$$h_c = 3.3\, v_w + 6.5 \quad (2)$$

$$h_c = 9.5\, v_w^{0.48} \quad (3)$$

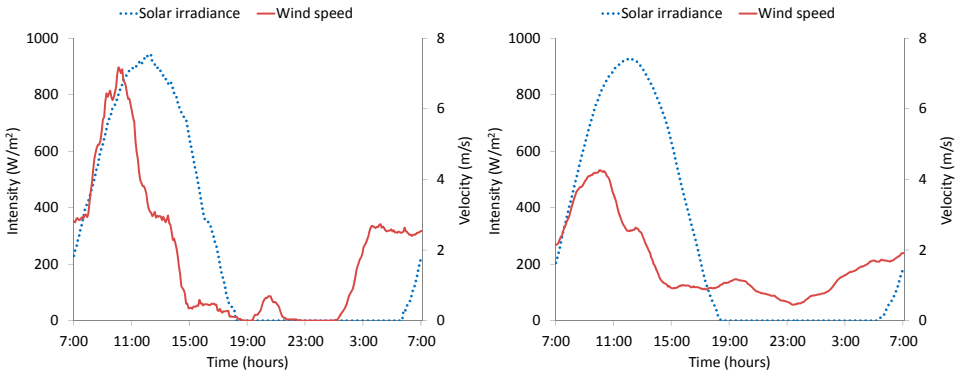

Figure 5. Global solar radiation intensity (G) and wind speed (v_w) for (**A**) the sample day and (**B**) average of the 14 days.

3.2. Temperature Drop

The measured front surface temperatures of the reference block A ($T_{\alpha f}$), block B ($T_{\beta f}$), block C ($T_{\gamma f}$) and the ambient temperature (T_{amb}) for the sample day and average of the 14 days are presented in Figure 6A,B, respectively. Figure 6A shows that the T_{amb} started at 35 °C and increased afterwards with a stable gradient to the peak value of 50.7 °C at 15:35. The T_{amb} stayed above 42 °C (upper limit of the PCM melting range) for 10.3 h, indicating a sufficient time for PCM to get melted by the ambient heat. The T_{amb} started to drop at 16:35 and reached the minimum value of 32 °C at 05:50. At nighttime, the T_{amb} stayed below PCM solidus temperature of 37 °C for 9.8 h (sufficient time to get solidified), while during the daytime it stayed above PCM liquidus temperature of 42 °C for 10.3 h (sufficient time to get melted). This shows that the PCM melting point is optimal for melting during daytime and solidification during nighttime.

The effect of inclusion of the PCM in the concrete blocks can be observed by comparing temperatures at the front surface of the three blocks, A ($T_{\alpha f}$), B ($T_{\beta f}$) and C ($T_{\gamma f}$). At the start, the three temperatures were almost the same (34 °C), however, as the day progressed, the $T_{\beta f}$ and the $T_{\gamma f}$ showed a decrement and time lag compared to the $T_{\alpha f}$. The observed decrement and time lag in $T_{\beta f}$ and $T_{\gamma f}$ can be attributed to the cooling effect produced by the PCM contained in the blocks B and C, respectively. A similar trend in the evolution of temperatures can be observed for the average of the 14 days, with relatively smoother curves as shown in Figure 6B. The temperature drop yielded by block B and block C ($T_{\beta f}$ and $T_{\gamma f}$) compared to the reference block A ($T_{\alpha f}$) is presented in the inset windows of Figure 6A,B. The temperature drop is negligible at the start of the experiment, however, it increased gradually reaching the peak value of 2.3 °C and 4.1 °C for blocks B and C, respectively at 15:10. Block C achieved higher cooling during daytime compared to block B mainly due to the placement location of the PCM. In the case of block C, the PCM layer was placed closer to the outer concrete layer, while in the case of block B, the PCM was placed closer to the inner concrete layer. Both the arrangements have an air cavity in proximity for natural ventilation. This highlights that placement of the PCM layer can be an important consideration while integrating PCM into buildings, depending on whether heat needs to be retained (cold climate) or removed (hot climate) [20,28]. After 16:00, the temperature difference started decreasing and became negative at 22:20, as shown in the window graph of Figure 6A,B. The window graphs present the difference of the front surface temperatures of block B ($Diff\ T_{\beta f} = T_{\alpha f} - T_{\beta f}$) and C ($Diff\ T_{\gamma f} = T_{\alpha f} - T_{\gamma f}$) to those of the reference block A. The negative temperature drop at night shows a slower self-cooling of blocks B and C (due to higher heat retention) compared to block A [39]. Heat absorbed in the PCM can be circulated indoors in a colder climate (or winter season) to reduce heating load [40]. In a hot climate, the challenge posed is to discard the heat absorbed by the PCM to regenerate the PCM to solid and avoid overheating in the building [41].

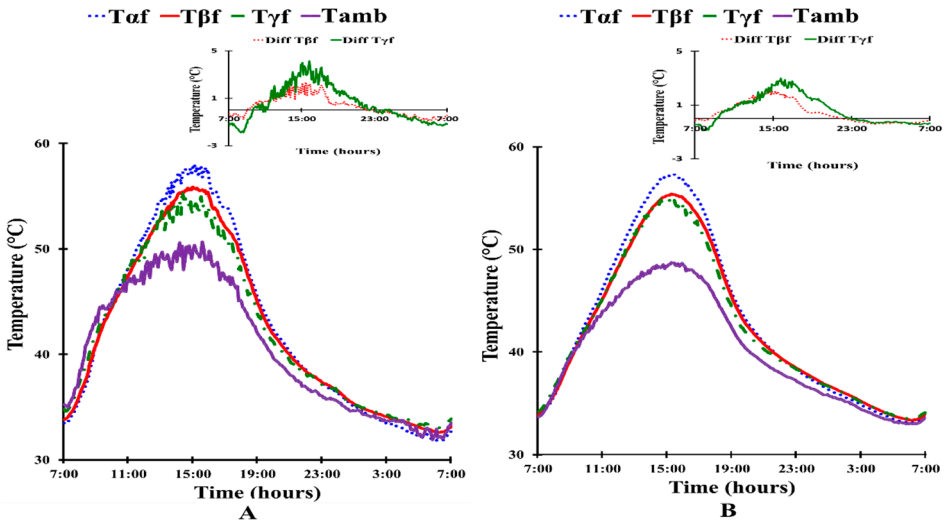

Figure 6. Evolution of the front surface temperature of reference block A ($T_{\alpha f}$), block B ($T_{\beta f}$) and block C ($T_{\gamma f}$), along with T_{amb} for (**A**) the sample day and (**B**) average of the 14 days, while the difference of the front surface temperatures of blocks B and C from the reference block A are presented in the corresponding inset graphs.

Heat absorbed in the PCM resulted in reduced heat transfer to the interior layers, which rendered a drop in the back surface temperatures of blocks B ($T_{\beta b}$) and C ($T_{\gamma b}$) compared to block A ($T_{\alpha b}$), presented in Figure 7. The $T_{\alpha b}$, $T_{\beta b}$ and $T_{\gamma b}$ were 33 °C, 33 °C and 36 °C, respectively, at the start of the experiment, as shown in Figure 7A. The three temperatures differed in the subsequent transient temperature rise, with the peak values of 52.4 °C, 50.7 °C and 48.3 °C, respectively. The $T_{\gamma b}$ was higher at the start of the experiment due to higher heat retention in block C compared to blocks A and B [40] on the previous night. The window graphs in Figure 7 present the difference of the back surface temperatures of blocks B ($Diff\ T_{\beta b} = T_{\alpha b} - T_{\beta b}$) and C ($Diff\ T_{\gamma b} = T_{\alpha b} - T_{\gamma b}$) with respect to the reference block A. A temperature drop of 4.5 °C at the back surface is achieved at the peak time in blocks B and C compared to block A. The average temperature rise for the 14 days presented in Figure 7B shows a similar profile as well. It is observed that block C generally achieved a higher temperature drop during daytime (5 °C at the peak) compared to block B (4 °C at the peak), however, the trend reversed at nighttime. The lower temperature achieved by block B at night can be explained by the relative positioning of the insulation, the PCM and the concrete layers in the two blocks. In the case of block B, the insulation layer adjacent to the indoor air retained minimum heat due to a lesser thermal mass and thereby transmits more heat to indoors during the daytime, yielding less temperature drop. At nighttime, the opposite happened, as the insulation layer retained the least amount of heat to transmit indoors, thereby achieving higher temperature drop. In block C, the concrete layer adjacent to the indoors retained more heat during daytime and reduced heat transmission indoors, achieving higher temperature drop. At night, however, the stored heat was released to the indoors, thereby increasing indoors temperature and yielding a negative temperature difference compared to the reference. This, therefore, emphasizes that although block C achieved better cooling during daytime and at peak, it cannot sufficiently discard the absorbed heat to the outdoor ambient through natural convection and would need additional mechanical ventilation for better overall performance.

The reduced back surface temperatures resulted in a drop in indoor temperature in the test chambers B ($T_{\beta i}$) and C ($T_{\gamma i}$), compared to the test chamber A ($T_{\alpha i}$), as shown in Figure 8A,B. The window graphs in Figure 8 present the difference of the indoor temperatures of chambers B ($Diff\ T_{\beta i} = T_{\alpha i} - T_{\beta i}$) and C ($Diff\ T_{\gamma i} = T_{\alpha i} - T_{\gamma i}$) with respect to the reference. At the start, the temperature in the test chamber C ($T_{\gamma i}$) was higher than that of the test chambers A ($T_{\alpha i}$) and B ($T_{\beta i}$) mainly due to heat transmitted by the concrete layer during the previous night. It was observed that

chambers B and C started to lag in temperature by 0.3 h and 1 h, respectively, compared to chamber A, with the peak values of 51.6 °C, 50.8 °C and 49.4 °C, respectively. The temperature drop in chambers B and C with respect to the reference chamber A is plotted in inset Figure 8A,B. According to the inset graph of Figure 8B, the difference was negative at the start of the experiment and became positive at 08:50 for both of the configurations. Chamber B yielded generally a lower temperature drop with a maximum value of 1.4 °C, nevertheless, it stayed positive for most of the day and night. Chamber C rendered a higher temperature drop, with the peak value of 3.1 °C, however, it stayed positive mainly during the daytime up to 12 h. The configuration of chambers B and C achieved a 5.4% and 8.5% higher cooling effect indoors on average, respectively, compared to the reference chamber A during the daytime.

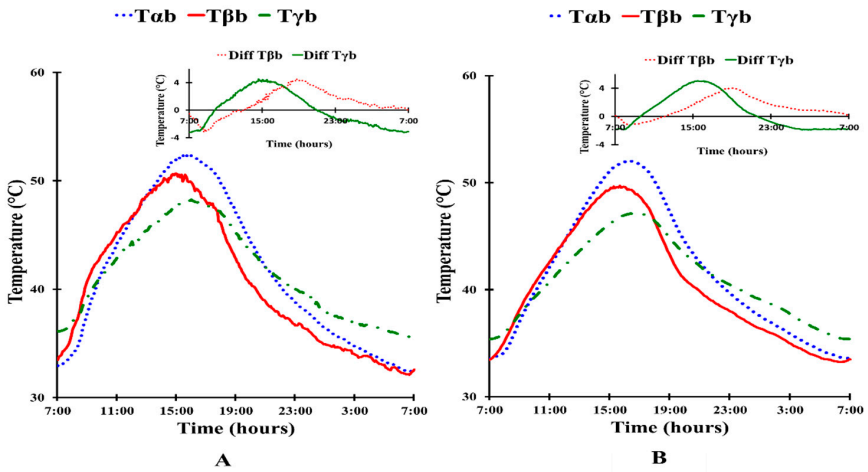

Figure 7. Evolution of the back surface temperatures of the reference block A ($T_{\alpha b}$), block B ($T_{\beta b}$) and block C ($T_{\gamma b}$) for (**A**) the sample day and (**B**) average of the 14 days, while the difference of the back surface temperatures of test blocks B and C from the reference block are presented in the corresponding inset graphs.

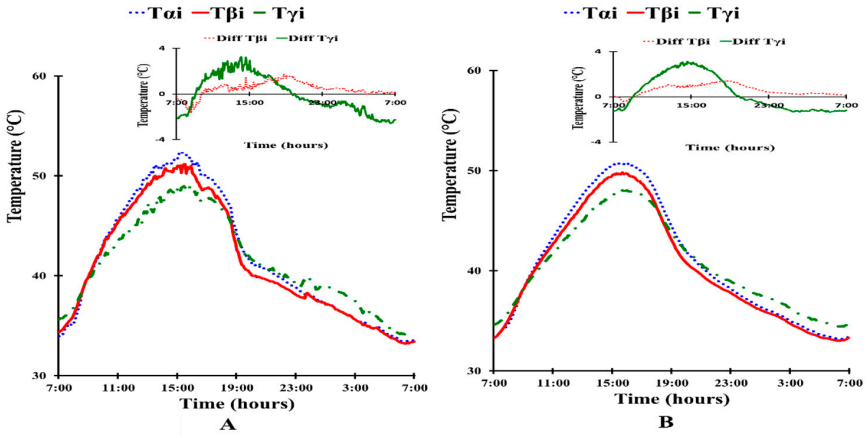

Figure 8. Evolution of the indoor temperature for the reference chamber A ($T_{\alpha i}$), chamber B ($T_{\beta i}$) and chamber C ($T_{\gamma i}$) for (**A**) the sample day and (**B**) average of the 14 days while the difference of the indoor temperatures of the test chambers B and C from the reference chamber are presented in the corresponding inset graphs.

Table 2 contains a summary of the solar radiation intensity (G), wind speed (v_w), ambient temperature (T_{amb}), temperatures at the front surfaces ($T_{\alpha f}$, $T_{\beta f}$ and $T_{\gamma f}$), temperatures at the back surfaces ($T_{\alpha b}$, $T_{\beta b}$ and $T_{\gamma b}$) and air temperature indoors ($T_{\alpha i}$, $T_{\beta i}$ and $T_{\gamma i}$) for the 14 days of the experiment with mean, standard deviation (SD) and coefficient of variation (CV).

Table 2. Summary of the weather data, temperatures of the blocks A, B and C and the indoor temperatures for the consecutive 14 days with statistical analysis.

Days		1	2	3	4	5	6	7	8	9	10	11	12	13	14	Mean	SD [1]*	CV [2]*
G	Total (Wh/day)	717	713	679	713	740	722	704	727	709	705	727	717	719	711	709	14	1.9%
	Max. (Wm^{-2})	944	917	907	922	980	950	919	975	907	914	958	950	939	934	944	23	2.5%
v_w (m/s)	Max.	7.2	6.1	5.2	5.3	4.1	5.3	5.3	3.6	3.4	3.3	3.5	5.6	5.7	5.1	5.2	1.1	21.4%
	Avg.	1.9	1.6	2.1	2.3	1.8	1.8	1.6	1.1	1.2	1.1	1.5	2.0	1.9	1.2	1.7	0.4	21.8%
T_{amb} (°C)	Max.	50.7	50.6	51.1	48.9	48.8	48.2	48.8	50.7	50.6	50.6	49.7	49.1	49.7	51.0	49.6	0.9	1.9%
	Min.	31.9	32.3	31.5	30.9	31.1	31.2	33.1	33.0	32.9	33.1	34.0	33.9	33.7	33.2	32.4	1.0	3.2%
	Avg.	40.6	40.5	39.7	38.5	38.5	38.2	40.0	41.2	40.8	41.1	40.9	40.3	40.3	41.2	39.7	1.0	2.5%
$T_{\alpha f}$ (°C)	Max.	58.0	58.2	58.1	56.8	56.5	56.4	56.6	59.3	57.7	58.9	58.0	57.0	57.9	59.9	58.1	1.0	1.8%
	Avg.	42.6	43.1	42.7	41.5	41.3	41.4	42.6	43.5	43.2	43.9	43.7	43.0	42.9	43.7	42.6	0.8	1.9%
$T_{\beta f}$ (°C)	Max.	55.9	55.8	56.1	54.3	54.0	53.8	54.3	57.1	55.5	56.9	56.2	55.0	55.6	57.8	55.8	1.2	2.1%
	Avg.	42.3	42.7	42.4	41.0	40.8	40.8	42.3	43.1	42.7	43.4	43.3	42.5	42.5	43.2	42.1	0.9	2.1%
	Diff.	2.3	2.5	2.2	2.8	2.5	2.7	2.5	2.6	2.2	2.1	2.2	2.3	2.6	2.3	2.5	0.2	8.3%
$T_{\gamma f}$ (°C)	Max.	55.6	55.4	56.4	54.2	54.5	53.8	54.9	56.8	56.5	57.7	56.7	56.4	56.3	58.6	56.2	1.3	2.3%
	Avg.	42.1	42.4	41.8	40.7	40.5	40.5	42.0	42.9	42.6	43.4	43.2	42.4	42.3	43.4	41.9	1.0	2.3%
	Diff	4.1	4.3	3.9	4.5	4.1	4.7	4.7	4.1	3.3	4.2	3.7	3.6	3.7	3.6	4.0	0.4	10.2%
$T_{\alpha b}$ (°C)	Max.	52.4	52.7	52.8	51.5	50.7	50.9	51.1	53.2	52.0	53.4	52.7	51.4	52.1	54.3	52.5	1.0	1.9%
	Avg.	41.6	41.9	41.4	40.2	40.1	40.0	41.5	42.5	42.1	42.6	42.7	41.9	41.8	42.6	41.1	0.9	2.2%
$T_{\beta b}$ (°C)	Max.	50.7	50.4	51.0	49.2	48.4	48.3	48.6	51.2	50.2	50.9	50.3	49.3	49.7	51.4	49.9	1.0	2.0%
	Avg.	40.5	40.8	40.1	38.8	38.8	38.6	40.3	41.4	41.1	41.5	41.3	40.6	40.6	41.4	40	1.0	2.4%
	Diff.	4.5	4.2	4.6	4.6	4.6	5.6	4.0	5.0	4.2	4.4	4.3	4.0	4.3	5.0	4.6	0.4	9.3%
$T_{\gamma b}$ (°C)	Max.	48.3	48.3	48.0	46.5	45.9	45.4	46.3	47.9	47.6	47.3	47.3	47.0	47.3	49.1	47.2	1.0	2.1%
	Avg.	41.5	41.7	41.0	39.7	39.6	39.2	40.7	41.6	41.1	41.3	41.6	41.0	41.2	42.1	40.6	0.8	2%
	Diff	4.5	4.7	5.3	5.2	5.0	5.7	5.2	5.8	4.7	6.3	5.6	4.6	5.1	5.6	5.1	0.5	9.7%
$T_{\alpha i}$ (°C)	Max.	51.6	51.3	51.9	50.4	49.5	49.6	50.0	52.7	51.6	52.2	51.6	50.6	50.8	53.1	51.3	1.1	2.1%
	Avg.	40.9	41.1	40.5	39.4	39.3	39.2	40.7	41.8	41.6	42.0	41.9	41.1	41.1	41.9	40.6	0.9	2.3%
$T_{\beta i}$ (°C)	Max.	50.8	50.6	51.1	49.4	48.4	48.3	48.7	51.2	50.4	51.1	50.3	49.4	49.6	51.3	49.8	1.0	2.0%
	Avg.	40.4	40.7	40.0	38.7	38.7	38.5	40.1	41.3	41.0	41.3	41.2	40.5	40.5	41.3	39.9	1.0	2.4%
	Diff.	1.7	1.6	1.6	1.9	1.8	2.1	1.7	2.4	2.1	2.8	1.9	2.1	2.1	2.5	2.2	0.3	15.5%
$T_{\gamma i}$ (°C)	Max.	49.4	49.3	49.0	47.7	46.8	46.5	47.3	49.2	48.6	48.2	48.3	47.9	48.0	49.6	48	1.0	2.0%
	Avg.	40.9	41.2	40.4	39.1	39.0	38.8	40.3	41.4	41.1	41.3	41.4	40.7	40.8	41.6	40.2	0.9	2.3%
	Diff	3.3	3.0	3.8	3.4	3.7	3.9	3.4	4.2	3.7	4.4	3.9	3.2	3.5	3.9	3.7	0.4	10.2%

[1]*—Population standard deviation; [2]*—coefficient of variation.

3.3. Reduction in Heat Gain

The reduction in heat gain by the blocks containing PCM was calculated by comparing the resulting indoor temperatures by each configuration given by Equation (4).

$$Q = h_c \times A \times (T_b - T_i) \quad (4)$$

where Q is the heat transfer rate from the back surface to indoors, h_c is the convective heat transfer coefficient (between the back surface and the indoors in this case), T_b is the back surface temperature and T_i is the indoor air temperature. The h_c value at the back surface facing indoors was found to be 6.5 W/m^2·K, calculated by assuming free cooling, employing zero air velocity in Equation (2). Cooling load saving is calculated by the difference of heat transfer rates between the back surface and the indoors for the reference (A) and the blocks containing the PCM (B and C). Figure 9 shows that block B, with the PCM layer closer to the interior, achieves a higher reduction in heat transfer compared to block C, with the PCM closer to the outer layer. The reduction in the heat transfer on 24 h balance was 137 Wh/m^2 and 32 Wh/m^2 for block B the block C, respectively. The heat gain reduction was 44% by the block B and 10.5% by the block C on 24 h basis compared to the block A. The results were found to be in agreement with the previously reported literature findings [26,27]. In [26], a PCM-integrated, building-integrated photovoltaic system reduced roof-generated heating loads by 30% in the winter and cooling load by 55% in the summer. In [27], a wall outfitted with a PCM reduced space-cooling load by 10.4%.

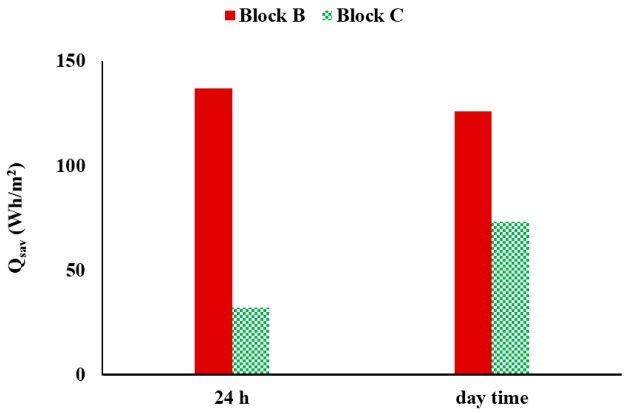

Figure 9. Average cooling load reduction achieved by block B and block C compared to the reference block A for 24 h and for daytime only.

3.4. Research Limitations

The research and findings have following limitations:

(1) The experiments were carried out in the peak summer conditions and are limited to 14 days only. Although the prevalent weather in Al Ain is hot, there are months that are mild to cool. Therefore, the net heat gain prevented in the peak of summer is expected to drop when aggregated for the whole year.
(2) The experiments were conducted without studying leakage of the PCM over repeated cycles at the time scale of a year. This will be an important consideration for future research.
(3) Natural or forced convection heat removal from the air cavity is not incorporated in the research, undermining the PCM re-solidification.
(4) The scale of the experiment is very small and would be less representative of a building.
(5) The authors plan to address all the stated limitations in future research.

4. Conclusions

Concrete blocks containing PCM (blocks B and C) in two different arrangements—by relocating PCM and insulation layers—were investigated to compare their cooling performance with a block without PCM (the block A). The inclusion of the PCM reduced heat transmission to indoors by 44% (block B) and 10.5% (block C) at 24 h energy balance and delayed the peak temperature by 2.6 h at the maximum. Block B remained cooler compared to the reference block A during daytime and most of the nighttime. Block C remained cooler than the reference block A during daytime and warmer during nighttime. Both the PCM inclusion arrangements, however, prevented 137 Wh/m^2 and 32 Wh/m^2 heat transmission based on 24 h energy balance for block B and block C, respectively. In the current research, the PCM is passively cooled by an airflow cavity without mechanical ventilation. The current research finds that passive heat removal from PCM through natural ventilation alone is insufficient in hot climates even with a higher PCM solidus temperature (37 °C), which limits the PCM performance. Future research will investigate active means for removing the heat retained in the PCM. The design will involve linking the air stream through the cavity wall containing PCM to the air circuitry in the air conditioning system.

Acknowledgments: The authors would like to express their appreciation to United Arab Emirates University (UAEU) for funding the research through National Research Foundation (NRF-31N103) and Program for Advanced Research (31N204). The authors would also extend thanks to the Faculty of Engineering at UAE University for the support to conduct experimentation.

Author Contributions: Ahmad Hasan and Khaled A. Al-Sallal conceived and designed the experiments; Ahmad Hasan and Hamza Alnoman performed the experiments; Yasir Rashid analyzed the data; Shaimaa Abdelbaqi contributed in data acquisition; Yasir Rashid wrote the paper.

Conflicts of Interest: The authors declare no conflict of interest.

Nomenclature

A	Surface area of the concrete block (m^2)
CV	Coefficient of variation (%)
G	Global solar radiation intensity incident on the surface (W/m^2)
h_c	Convective heat transfer coefficient ($W/m^2 \cdot K$)
HVAC	Heating, ventilation & air conditioning
m	Mass of the concrete block (kg)
PCM	Phase change material
Q	Heat transfer rate (W/m^2)
Q_{in}	Incident solar energy (Wh/m^2)
SD	Population standard deviation
T	Temperature (°C)
t	time (h)
v_w	Wind speed (m/s)
Subscripts	
α	Reference block A
β	Block B
γ	Block C
f	Front surface
b	Back surface
i	Indoor air

References

1. International Energy Agency. *Key World Energy Statistics 2014*; Chirat: Paris, France, 2014.

2. U.S. Greenhouse Gas Inventory Report: 1990–2014. US Environmental Protection Agency. Available online: http://www.epa.gov/climatechange/emissions/usinventoryreport.html (accessed on 16 September 2016).
3. Directive 2010/31/eu of the European Parliament and of the Council of 19 May 2010 on the Energy Performance of Buildings. Available online: http://eur-lex.europa.eu/LexUriServ/LexUriServ.do?uri=OJ:L:2010:153:0013:0035:EN:PDF (accessed on 16 September 2016).
4. U.S. Energy Information Administration. Issues in International Energy Consumption Analysis: Canadian Energy Demand. Available online: https://www.eia.gov/analysis/studies/international/consumption/pdf/canadian_resconsump.pdf (accessed on 16 September 2016).
5. U.S. Environmental Protection Agency. *Draft Inventory of U.S. Greenhouse Gas Emissions and Sinks: 1990–2014*; Environmental Protection Agency: Washington, DC, USA, 2016.
6. UK Building Regulations and EU Directives. *Zero Carbon Homes and Nearly zero Energy Buildings*; Zero Carbon Hub: London, UK, 2014.
7. Ulgen, K. Experimental and theoretical investigation of effects of wall's thermophysical properties on time lag and decrement factor. *Energy Build.* **2002**, *34*, 273–278. [CrossRef]
8. Kontoleon, K.J.; Bikas, D.K. The effect of south wall's outdoor absorption coefficient on time lag, decrement factor and temperature variations. *Energy Build.* **2007**, *39*, 1011–1018. [CrossRef]
9. Asan, H. Numerical computation of time lags and decrement factors for different building materials. *Build. Environ.* **2006**, *41*, 615–620. [CrossRef]
10. Di Perna, C.; Stazi, F.; Casalena, A.U.; D'Orazio, M. Influence of the internal inertia of the building envelope on summertime comfort in buildings with high internal heat loads. *Energy Build.* **2011**, *43*, 200–206. [CrossRef]
11. Aste, N.; Angelotti, A.; Buzzetti, M. The influence of the external walls thermal inertia on the energy performance of well insulated buildings. *Energy Build.* **2009**, *41*, 1181–1187. [CrossRef]
12. De Gracia, A.; Cabeza, L.F. Phase change materials and thermal energy storage for buildings. *Energy Build.* **2015**, *103*, 414–419. [CrossRef]
13. Raja, I.A.; Nicol, J.F.; McCartney, K.J.; Humphreys, M.A. Thermal comfort: Use of controls in naturally ventilated buildings. *Energy Build.* **2001**, *33*, 235–244. [CrossRef]
14. Zhou, D.; Zhao, C.Y.; Tian, Y. Review on thermal energy storage with phase change materials (PCMs) in building applications. *Appl. Energy* **2012**, *92*, 593–605. [CrossRef]
15. Evers, A.C.; Medina, M.A.; Fang, Y. Evaluation of the thermal performance of frame walls enhanced with paraffin and hydrated salt phase change materials using a dynamic wall simulator. *Build. Environ.* **2010**, *45*, 1762–1768. [CrossRef]
16. Fang, Y. A Comprehensive Study of Phase Change Materials (PCMs) for Building Walls Applications. Ph.D. Thesis, University of Kansas, Lawrence, KS, USA, 9 March 2009.
17. Mathieu-Potvin, F.; Gosselin, L. Thermal shielding of multilayer walls with phase change materials under different transient boundary conditions. *Int. J. Ther. Sci.* **2009**, *48*, 1707–1717. [CrossRef]
18. Diaconu, B.M.; Cruceru, M. Novel concept of composite phase change material wall system for year-round thermal energy savings. *Energy Build.* **2010**, *42*, 1759–1772. [CrossRef]
19. Huang, M.J.; Eames, P.C.; Hewitt, N.J. The application of a validated numerical model to predict the energy conservation potential of using phase change materials in the fabric of a building. *Sol. Energy Mater. Sol. Cells* **2006**, *90*, 1951–1960. [CrossRef]
20. Lee, K.O.; Medina, M.A.; Raith, E.; Sun, X. Assessing the integration of a thin phase change material (PCM) layer in a residential building wall for heat transfer reduction and management. *Appl. Energy* **2015**, *137*, 699–706. [CrossRef]
21. Jin, X.; Medina, M.A.; Zhang, X. On the placement of a phase change material thermal shield within the cavity of buildings walls for heat transfer rate reduction. *Energy* **2014**, *73*, 780–786. [CrossRef]
22. Selka, G.; Korti, A.N.; Abboudi, S. Dynamic thermal behavior of building using phase change materials for latent heat storage. *Therm. Sci.* **2014**, *19*, 134. [CrossRef]
23. Soares, N.; Gaspar, A.R.; Santos, P.; Costa, J.J. Experimental evaluation of the heat transfer through small PCM-based thermal energy storage units for building applications. *Energy Build.* **2016**, *116*, 18–34. [CrossRef]
24. Royon, L.; Karim, L.; Bontemps, A. Thermal energy storage and release of a new component with PCM for integration in floors for thermal management of buildings. *Energy Build.* **2013**, *63*, 29–35. [CrossRef]

25. Soares, N.; Samagaio, A.; Vicente, R.; Costa, J. Numerical simulation of a PCM shutter for buildings space heating during the winter. In Proceedings of the World Renewable Energy Congress-Sweden, Linköping, Sweden, 8–13 May 2011; Linköping University Electronic Press: Linköping, Sweden; pp. 1797–1804.
26. Kośny, J.; Biswas, K.; Miller, W.; Kriner, S. Field thermal performance of naturally ventilated solar roof with PCM heat sink. *Sol. Energy* **2012**, *86*, 2504–2514. [CrossRef]
27. Lee, K.O.; Medina, M.A. Using phase change materials for residential air conditioning peak demand reduction and energy conservation in coastal and transitional climates in the State of California. *Energy Build.* **2016**, *116*, 69–77. [CrossRef]
28. Campbell, K.R.; Sailor, D.J. Phase change materials as thermal storage for high performance homes. In Proceedings of the ASME 2011 International Mechanical Engineering Congress and Exposition, Denver, CO, USA, 11–17 November 2011; pp. 809–818.
29. Heim, D.; Wieprzkowicz, A. Positioning of an isothermal heat storage layer in a building wall exposed to the external environment. *J. Build. Perform. Simul.* **2016**. [CrossRef]
30. Evola, G.; Marletta, L.; Sicurella, F. Simulation of a ventilated cavity to enhance the effectiveness of PCM wallboards for summer thermal comfort in buildings. *Energy Build.* **2014**, *70*, 480–489. [CrossRef]
31. Neeper, D.A. Thermal dynamics of wallboard with latent heat storage. *Sol. Energy* **2000**, *68*, 393–403. [CrossRef]
32. Heim, D.; Clarke, J.A. Numerical modelling and thermal simulation of PCM–gypsum composites with ESP-r. *Energy Build.* **2004**, *36*, 795–805. [CrossRef]
33. Hasan, A.; McCormack, S.J.; Huang, M.J.; Norton, B. Characterization of phase change materials for thermal control of photovoltaics using Differential Scanning Calorimetry and Temperature History Method. *Energy Convers. Manag.* **2014**, *81*, 322–329. [CrossRef]
34. Hasan, A.; Alnoman, H.; Rashid, Y. Impact of integrated photovoltaic-phase change material system on building energy efficiency in hot climate. *Energy Build.* **2016**, *130*, 495–505. [CrossRef]
35. Rubitherm. Available online: http://www.rubitherm.eu/media/products/datasheets/Techdata_-RT42_EN_09052016.PDF (accessed on 5 August 2016).
36. Apogee Instruments. Specification Sheet. Available online: http://www.apogeeinstruments.co.uk/content/SP-100-200-spec-sheet.pdf (accessed on 5 August 2016).
37. National Instruments. Available online: http://sine.ni.com/nips/cds/view/p/lang/en/nid/205621 (accessed on 5 August 2016).
38. Sharples, S.; Charlesworth, P.S. Full-scale measurements of wind-induced convective heat transfer from a roof-mounted flat plate solar collector. *Sol. Energy* **1998**, *62*, 69–77. [CrossRef]
39. Cabeza, L.F.; Castellon, C.; Nogues, M.; Medrano, M.; Leppers, R.; Zubillaga, O. Use of microencapsulated PCM in concrete walls for energy savings. *Energy Build.* **2007**, *39*, 113–119. [CrossRef]
40. Zhou, G.; He, J. Thermal performance of a radiant floor heating system with different heat storage materials and heating pipes. *Appl. Energy* **2015**, *138*, 648–660. [CrossRef]
41. Hasan, A.; McCormack, S.J.; Huang, M.J.; Sarwar, J.; Norton, B. Increased photovoltaic performance through temperature regulation by phase change materials: Materials comparison in different climates. *Sol. Energy* **2015**, *115*, 264–276. [CrossRef]